LHON Gene Therapy Vector Prevents Visual Loss and Optic Neuropathy Induced by G11778A Mutant Mitochondrial DNA: Biodistribution and Toxicology Profile

Rajeshwari Koilkonda,[1] Hong Yu,[1] Venu Talla,[1] Vittorio Porciatti,[1] William J. Feuer,[1] William W. Hauswirth,[2] Vince Chiodo,[2] Kirsten E. Erger,[3] Sanford L. Boye,[2] Alfred S. Lewin,[4] Thomas J. Conlon,[3] Lauren Renner,[5] Martha Neuringer,[5] Carol Detrisac,[6] and John Guy[1]

[1]Bascom Palmer Eye Institute, University of Miami, Miller School of Medicine, Miami, Florida, United States
[2]Department of Ophthalmology, University of Florida, College of Medicine, Gainesville, Florida, United States
[3]Department of Pediatrics, University of Florida, College of Medicine, Gainesville, Florida, United States
[4]Department of Molecular Genetics and Microbiology, University of Florida, College of Medicine, Gainesville, Florida, United States
[5]Oregon National Primate Research Center, Oregon Health and Science University, Beaverton, Oregon, United States
[6]Charles River Pathology Associates-Illinois, Chicago, Illinois, United States

Correspondence: John Guy, Neuro-Ophthalmology Service, Bascom Palmer Eye Institute, McKnight Building Room 404, 1638 NW 10th Avenue, Miami, FL 33136, USA; jguy@med.miami.edu.

Submitted: August 3, 2014
Accepted: October 13, 2014

Citation: Koilkonda R, Yu H, Talla V, et al. LHON gene therapy vector prevents visual loss and optic neuropathy induced by G11778A mutant mitochondrial DNA: biodistribution and toxicology profile. *Invest Ophthalmol Vis Sci*. 2014;55:7739–7753. DOI:10.1167/iovs.14-15388

Purpose. To demonstrate safety and efficacy of allotopic human ND4 for treatment of a Leber's hereditary optic neuropathy (LHON) mouse model harboring the G11778A mitochondrial mutation.

Methods. We induced LHON in mice by intravitreal injection of mutant (G11778A) human ND4 DNA, responsible for most cases of LHON, that was directed to mitochondria using an AAV2 vector to which we appended a mitochondrial targeting sequence to the VP2 capsid. We then attempted rescue of visual loss using our test article (ScAAV2-*P1ND4v2*) containing a synthetic nuclear encoded G11778G ND4 gene that was allotopically expressed. Control mice either were uninjected or received AAV2-*GFP* or AAV2-*mCherry*. We performed RT-PCR and confocal microscopy at 2 weeks post injection. Pattern electroretinograms (PERGs), spectral-domain optical coherence tomography (SD-OCT), histology, and transmission electron microscopy (TEM) were performed. For toxicology and biodistribution studies, the test article was administered intravitreally to rats and rhesus macaques at different doses.

Results. Mutant and wild-type ND4 were efficiently expressed in the mitochondria of retinal ganglion cells (RGCs). Visual function assessed by serial PERGs and retinal structure by serial SD-OCT showed a significant rescue by the test article. Histology and ultrastructural analysis confirmed that loss of RGCs and demise of axons was prevented by ScAAV2-*P1ND4v2*. Rat and nonhuman primate biodistribution studies showed that vector spread outside the injected eye into spleen and lymph nodes was minimal. Histopathology of tissues and organs including the eyes was comparable to that of uninfected and saline-injected eyes.

Conclusions. Allotopically expressed wild-type ND4 prevents the phenotype induced by G11778A mitochondrial DNA with a toxicology profile acceptable for testing in a phase I clinical trial.

Keywords: LHON, mitochondria, gene therapy

The field of human mitochondrial genetics was born a quarter-century ago, and the list of neurodegenerative disorders associated with mutated mitochondrial DNA keeps growing. While many different experimental approaches have been proposed, development of a clinically effective therapy has been elusive.[1] Leber's hereditary optic neuropathy (LHON) is a maternally inherited disease, first described in 1871, resulting in acute bilateral and permanent loss of central vision usually in the second and third decades of life. In approximately 95% of patients, it is caused by three pathogenic point mutations in respiratory chain subunits of nicotinamide adenine dinucleotide-ubiquinone-oxidoreductase that is complex 1. They include a G to A transition at nucleotide 3460 in ND1 or at nucleotide 11778 in ND4 or a T to C transition in nucleotide 14484 in ND6 of the approximately 16-kb mitochondrial genome. In most LHON patients with visual loss, the pathogenic mitochondrial DNA (mtDNA) mutations are homoplasmic, that is, lacking normal mtDNA. However, approximately 14% of the patients may have the mutation in the heteroplasmic condition, that is, with both normal and mutated mtDNA.[2,3] Of the three mutations, the G11778A resulting in arginine to histidine substitution at amino acid 340 of ND4 (R340H) is responsible for half of the cases. Spontaneous visual improvement is rare and often incomplete.[2,4–7]

A potential target for therapeutic intervention is to introduce a normal copy of the defective ND4 allele into retinal ganglion cells (RGCs), the cell type exclusively affected in LHON. Replacing a defective gene has been the basis for more than 1500 gene therapy clinical trials worldwide, but only two involving mitochondrial disease (ClinicalTrials.gov No.

NCT01267422, located in China, and No. NCT02064569, located in France). One of the major drawbacks with treating mtDNA diseases by gene therapy has been a lack of availability of practical methods.[8,9] To address this question, we and other groups have investigated an alternative approach, "allotopic expression," in which a nuclear version of the mitochondrial gene (in this case ND4) was expressed in the nucleus, translated on cytoplasmic polyribosomes, and then imported into the mitochondria with the addition of an N-terminal mitochondrial targeting sequence.[10–12] Previously, our group reported that allotopic expression of the normal ND4 gene corrected the defective adenosine triphosphate (ATP) synthesis in LHON cells with homoplasmic G11778A mtDNA mutation.[13] We next delivered a nuclear-encoded version of mutant human ND4 (R340H) allele into the mouse visual system and were successful in generating a bona fide mouse LHON model. This mouse model not only exhibited disruption of mitochondrial architecture and increased generation of reactive oxygen species (ROS), but also had swelling of optic nerve head, following which RGCs showed apoptosis with a progressive demise including degeneration of axons comprising the optic nerve, the key hallmarks of LHON pathology.[14]

As viruses have been shown to enter mitochondria[15] and the normal AAV vector has been shown to deliver some of its DNA to mitochondria,[16] we created an LHON mouse model by a different approach. We efficiently redirected the AAV virion to mitochondria by adding a mitochondrial targeting sequence (MTS) to the viral capsid surrounding its DNA core. This cytochrome oxidase subunit 8 (COX8) presequence was fused in frame to the N-terminus of *GFP* in the AAV2 VP2 capsid open reading frame. The mutant G11778A human ND4 gene in the mitochondrial genetic code driven by the human mitochondrial heavy strand promoter (HSP) was packaged into this MTS-AAV and delivered to the visual system of mice. This approach resulted in transcription and translation of mutant human ND4 in mitochondria where it induced visual loss and optic atrophy.[17,18] We had previously shown that wild-type ND4 packaged into the MTS-AAV prevented visual loss and optic neuropathy induced by the mutant allotopic R340H ND4 allele.

In this study, we investigated if our proposed test article, ScAAV2-*P1ND4v2*, containing the human wild-type ND4 subunit gene of complex I that is expressed allotopically would prevent the LHON pathology of rodents generated by the MTS-AAV approach delivering the mutant ND4 allele to murine RGCs and their axons in the optic nerve. This scenario would be most analogous to the treatment of LHON patients in whom disease is induced by the mutant G11778A mtDNA. In this set of experiments, the ratio of mutant ND4 relative to test article (ScAAV-*P1ND4v2*) is 4:1, thus 16-fold less than the 4:1 ratio of ScAAV-*P1ND4v2* to mutant allotopic R340H ND4 described in our previous study of allotopic rescue of disease caused by an allotopic mutant R340H ND4. With mutant ND4 DNA in excess, we show that ScAAV2-*P1ND4v2* prevents visual loss and optic neuropathy induced by mutant G11778A DNA. We also performed additional safety experiments to demonstrate that ScAAV2-*P1ND4v2* does not spread outside the eye or cause any pathology in normal rodents and in nonhuman primates at the highest doses planned for the human phase I clinical trial.

Materials and Methods

Construction of the Viral Vector

The construct used in this study was designed to meet the needs for future human good manufacturing practices (GMP) vector usage. It was derived from the original fusion gene construct containing human nuclear encoded *ND4* with a MTS (ATP1) and a FLAG epitope tag, *P1ND4FLAG*-UF22-WRPE, which was previously described in detail.[19] For this study, the construct was modified to remove the FLAG tag. For this purpose, the *Xba*I digested fragment of *P1ND4FLAG*-UF22-WRPE was first cloned into the *Xba*I site of pBluescript II (Stratagene, La Jolla, CA, USA), resulting in plasmid pBS-*P1ND4* (*Xba*I). Self-complementary AAV vector plasmid, Sc-smCBA-*P1ND4,* was created by cutting Sc-trs-SB-smCBA-*hGFP* with *Bam*HI and *Not*I and ligating into the *Not*I and *Bam*HI fragment of pBS-*P1ND4* (*Xba*I). This Sc-AAV vector plasmid contained a promoter element, the 953 bp, and a truncated chimeric CMV/CBA promoter (smCBA) and had modifications in one of the AAV inverted terminal repeats that resulted in generation of self-complementary AAV genomes. These modifications were described in detail by McCarty and colleagues.[20] The resulting self-complementary plasmid containing smCBA driving *P1ND4-FLAG* was named Sc-smCBA-*P1ND4*. For the removal of extra polyadenylation signal and FLAG tag, Sc-smCBA-*P1ND4* was cut with *Sph*I and *Sal*I and ligated with a synthetic fragment of DNA with *Sph*I and *Sal*I ends. The *Sph*I/*Sal*I *P1ND4* fragment is a synthetic fragment of 1092 bases encompassing a *Sph*I site to the end of *P1ND4* cDNA with the 3′ end flanked by a *Sal*I site. This synthetic fragment was manufactured by Genscript (Piscataway, NJ, USA). The resulting construct from the ligation no longer contained the SV40 PolyA and 3′ FLAG epitope tag. The bGH polyA was already present in the vector plasmid progenitor and remains in the new construct. This new construct was named Sc-smCBA-*P1ND4v2*.

For inducing LHON disease in mice, we used AAV containing the human mitochondrial mutant *ND4* (G11778A) that was driven by the human mitochondrial HSP, ScAAV2-HSP-*ND4* (G11778A) FLAG. The human mutant *ND4* contained a stop codon AGA fused in frame downstream of the FLAG epitope. To the HSP-*ND4* (G11778A) FLAG construct, we added a second gene mitochondrial encoded (m) Cherry. In brief, nuclear encoded Cherry was cloned into pCDNA3 and was used as a template to generate a mitochondrial encoded gene with a substitution of A for C at 559 nt by site-directed mutagenesis (Quikchange II XL site-directed mutagenesis kit; Stratagene). After confirmation by DNA sequencing, the resultant cassette was cloned into the mutant HSP-mutant *ND4FLAG* backbone to give HSP-*ND4FLAG(G11778A)+m-Cherry*.

For delivery, we packaged both the allotopic wild-type and mutant *ND4* constructs into self-complementary AAV2 vectors with triple tyrosine (Y) to phenylalanine (F) modifications at positions 444, 500, and 730 (Y444F+Y500F+Y730F) in the VP3 capsid. The AAV containing mutant *ND4* was directed toward the mitochondria, using a MTS appended to the open reading frame of VP2. This MTS had a *GFP* sequence in frame, and the plasmid was designated COX8*GFP* VP2. For controls, *GFP* was packaged into self-complementary (sc) AAV2.

Animals

All animal procedures were performed in accordance with the National Institutes of Health Guide for the Care and Use of Laboratory Animals and the ARVO Statement for the Use of Animals in Ophthalmic and Vision Research.

Intraocular Injections (Mice and Rats)

For the intraocular injections of recombinant adeno-associated virus (rAAV), DBA/1J mice were sedated by inhalation with 1.5% to 2% isoflurane. A local anesthetic (proparacaine hydrochloride) was applied topically to the cornea, and a 32-

gauge needle attached to a Hamilton syringe (Hamilton Company, Reno, NV, USA) was inserted through the pars plana under the dissecting microscope (Carl Zeiss Microscopy, Thornwood, NY, USA). One microliter of ScAAV2-(Y444,500,730F)-HSP-*ND4 (G11778A)+mCherry* (COX8-GFP) (2.19×10^{12} particles/mL) ($n = 20$) was injected into the right and left eyes. Seventy-two hours after these injections, 1 μL of the test article, ScAAV2-(Y444,500,730F)-*P1ND4v2* (5.02×10^{11} particles/mL), was injected into 10 mice in both eyes (test group). The remaining 10 mice received 1 μL ScAAV2-*GFP* (4×10^{11} particles/mL) in both eyes (mock-treated group) or just ScAAV2-*mCherry* for the no-disease control group ($n = 6$). Another group of 10 mice were injected with the test article; 6 mice remained uninjected controls. Spraque-Dawley rats received intravitreal saline or *P1ND4v2* at doses of 6.56×10^6 ($n = 20$), 6.56×10^7 ($n = 20$), or 1.97×10^8 viral genomes (VG) ($n = 20$) or saline ($n = 20$).

Electrophysiology (Mice)

Pattern electroretinograms (PERGs) were obtained from mice ($n = 24$) at 2 months, 6 months, and 1 year after the viral injections. In brief, mice were weighed and anesthetized using intraperitoneal injections (0.5–0.7 mL/kg) of a mixture of ketamine (42.8 mg/mL) and xylazine (8.6 mg/mL) and were restrained using a bite bar and a nose holder that allowed unobstructed vision. The animals were kept at a constant body temperature of 37°C with a feedback-controlled heating pad (TCAT-2LV; Physitemp Instruments, Inc., Clifton, NJ, USA). Under these conditions, the eyes of mice were wide open and in a stable position, with undilated pupils pointing laterally and upward. The PERG electrode, with a diameter of 0.25 mm and made of silver wire configured to a semicircular loop of a 2-mm radius, was placed on the corneal surface by means of a micromanipulator and positioned to encircle the pupil without limiting the field of view. Reference and ground electrodes were stainless steel needles inserted under the skin of the scalp and tail, respectively. After setting the mice on the stage and before recording, a small drop of balanced salt solution was topically applied to the cornea to prevent drying. A visual stimulus of contrast-reversing (1 Hz, 2 reversals/s) horizontal bars was generated by a programmable graphic card (VSG; Cambridge Research Systems, Rochester, UK) on a cathode ray tube display (Multiscan 500; Sony, Boston, MA, USA) whose center was aligned with the projection of the pupil. Eyes were not refracted for the viewing distance because the mouse eye has a large depth of focus due to the pinhole pupil. At the viewing distance of 15 cm, the stimulus field covered an area of 69.4° × 63.4°. Patterns had a fixed mean luminance of 50 cd/m^2. Retinal signals were amplified (10,000-fold) and band-pass filtered (1–30 Hz). Three consecutive responses to 600 contrast reversals each were recorded. The responses were superimposed to check for consistency and then averaged (1800 sweeps). Averaged PERGs were automatically analyzed to evaluate the major positive and negative waves using commercially available software (SigmaPlot; Systat Software, Inc., San Jose, CA, USA). The waveform of averaged PERGs to high-contrast (1.0) gratings of low spatial frequency (0.05 cyc/deg) consisted of a major positive peak at around 90 to 120 ms (defined as P100) followed by a slower negative wave with a broad trough at around 200 to 300 ms. The maximal voltage in the expected time window for P100 (50–200 ms) and the minimal voltage in the expected time window for N250 (201–350 ms) were identified automatically using a simple macro written in SigmaPlot language (version 11.2). Statistical analysis was evaluated by *t*-test, and $P < 0.05$ was considered statistically significant.

Imaging (Mice)

In vivo high-resolution three-dimensional (3D) imaging of the mouse retina ($n = 26$) was performed at 4 months, 8 months, and 12 months post AAV injection using spectral-domain optical coherence tomography (SD-OCT; Bioptigen, Inc., Durham, NC, USA). Briefly, the mice were anesthetized with an intraperitoneal injection of ketamine (80 mg/kg) and xylazine (5 mg/kg). Both pupils were dilated with a topically applied drop of tropicamide (1%). To preserve corneal clarity, we applied a drop of Systane Ultra (Alcon Laboratories, Inc., Fort Worth, TX, USA) lubricating eye drops to the cornea. Mice were secured on a custom stage, which allowed free rotation, to align the eye for imaging of the optic nerve head (ONH). Rectangular volume scans centered on the ONH were acquired in both eyes with the Bioptigen SD-OCT system. For analysis of SD-OCT images, all data sets were checked to ensure that there was consistent image quality across the scan. Eyes with images showing shadowing due to the media opacities were excluded from analysis, as this could affect thickness measurements. A custom-made segmentation algorithm (Matlab; The Mathworks, Inc., Natick, MA, USA) was used to detect retinal boundaries and measure the distance from the nerve fiber layer (NFL) to the inner boundary of the inner nuclear layer (INL) for acquired images. The result of segmentation was used to calculate 3D thickness maps of the combined RGC+IPL layer. Statistical analysis was performed using Student's *t*-test; $P < 0.05$ was used as the cutoff for statistical significance.

For the detection of mitochondrial mCherry expression in mouse eyes, confocal scanning laser ophthalmoscopy (CSLO; Heidelberg Engineering, Bonn, Germany) imaging was performed 4 months following either inoculation with ScAAV2-*HSP-ND4(G11778A)+mCherry* along with test article ScAAV2-*P1ND4v2* ($n = 10$) or in mock-treated mice receiving Sc-AAV2-*GFP* ($n = 10$) or age-matched uninjected control ($n = 2$) ScAAV2-*GFP* injections. The built-in 488 laser was used for the excitation of both GFP and mCherry, and band-pass filters of 460 to 490 and 542 to 800 nm were used for the detection. For this purpose, the animals were anesthetized with ketamine/xylazine, pupils were dilated with phenylephrine/atropine, and corneal hydration was maintained with balanced salt solution. Retinal images were obtained using a 30° field of view and real-time averaging of 50 images. The CSLO was focused on the inner retina by imaging of the NFL at 488 nm through the CSLO polarization filter (red-free imaging).

Retina Cryosections and Immunolabeling (Mice)

For expression studies, mice were humanely killed 2 weeks after the viral injections ($n = 5$), and the eyes were removed and fixed with 4% paraformaldehyde in phosphate-buffered saline solution (PBS) for 1 hour. The eyes were then transferred to 0.4% paraformaldehyde overnight. To make flat mounts, the cornea and crystalline lens were removed, and the entire retina was carefully dissected from the eye cup. Four radial cuts were made from the edge to the equator of the retina to make it flat. After three washes in PBS, retinas were permeabilized with 0.5% Triton X-100 (Dow Chemical Corporation, Midland, MI, USA) in PBS for 1 hour followed by incubation with a blocking solution of 0.5% Triton X-100 and 10% goat serum for 1 hour. The flat-mounted retinas were then rinsed in PBS and incubated with a mixture of either mouse monoclonal anti-human ND4 antibody (Abnova, Taipei City, Taiwan) or mouse monoclonal anti-FLAG antibody (Sigma-Aldrich Corp., St. Louis, MO, USA), monoclonal rat Thy1.2 antibody (1:200; Abcam, Cambridge, MA, USA), or polyclonal rabbit anti-porin antibody (1:500; Abcam) overnight at 4°C. Primary antibody solution is contained in 10%

Investigative Ophthalmology & Visual Science

goat serum and 0.2% Triton X-100 in PBS (pH, 7.4). After three washes with PBS, retinas were reacted with the secondary antibody, goat anti-mouse Cy3 (Jackson Immunoresearch Laboratories, Inc., West Grove, PA, USA), goat anti-mouse FITC (Jackson Immunoresearch Laboratories, Inc.), goat anti-rat Cy2 (Jackson Immunoresearch Laboratories, Inc.), or goat anti-rabbit Cy5 (Jackson Immunoresearch Laboratories, Inc.), and 4′,6-diamidino-2-phenylindole (DAPI; 2 μg/mL) (Santa Cruz Biotechnology, Inc., Santa Cruz, CA, USA) in 1:500 dilution contained in 10% goat serum and 0.2% Triton X-100 and incubated at 4°C overnight. Retinal tissues were finally washed three times in PBS. Whole mounts were then placed on glass slides (RGC layer facing up), cover slipped, and observed for fluorescence with a confocal microscope (TCS SP5; Leica, Wetzlar, Germany). For cryosections, the retinas were incubated overnight in 30% sucrose and then embedded in optimal cutting temperature embedding compound (Sakura Finetek, Torrance, CA, USA). Retinal sections, 8 μm in thickness, were then mounted with fluorescent mounting medium (Vectashield; Vector Laboratories, Burlingame, CA, USA) and examined for fluorescence by confocal microscopy.

Histology and Ultrastructure (Mice)

For histology and electron microscopic analysis, mice receiving the dual viral injections were euthanized after 1 year ($n = 5$ animals in each group). Briefly, eyes and optic nerves of infected mice were dissected out after euthanasia and perfusion with fixative (4% paraformaldehyde, 2.5% glutaraldehyde) and were further processed by immersion fixation in 2.5% glutaraldehyde, postfixed in 1% osmium tetroxide, 0.1 M sodium cacodylate-HCl buffer (pH 7.4), 7% sucrose in the cold, and then dehydrated through an ethanol series to propylene oxide, infiltrated, and embedded in epoxy resin that was polymerized at 60°C overnight. Semithin longitudinal sections (0.5 μm) of the retina were stained with toluidine blue for light microscopic examination, and images were taken at 400× magnification. For quantification, cells in the RGC layer were counted. Ultrathin sections (90 nm) were placed on copper grids for examination with a Hitachi H-7600 unit (Hitachi, Tokyo, Japan) operating at 80 kV.

RT-PCR (Mice)

Total RNA was isolated from the retina, optic nerves, brain, liver, and pancreas at 2 weeks post injections using Trizol reagent (Invitrogen, Carlsbad, CA, USA) according to the manufacturer's directions ($n = 2$). First-strand cDNA was reverse transcribed from 1 μg total RNA in a final volume of 20 μL using reverse transcriptase and random hexamers from the iScript cDNA synthesis kit (Bio-Rad, Hercules, CA, USA). Polymerase chain reaction was performed using primers hND4-FP-5′ TGCTGAAGCTGGGCGGCTACGGC 3′ and hND4-RP-5′AACCGCCTCTCCCCGCGCGTT3′ with Taq DNA polymerase (Invitrogen) in a DNA Master cycler gradient (Eppendorf, Hauppauge, NY, USA) according to a standard protocol as follows: 1 cycle of 95°C for 3 minutes; 23 cycles of 94°C for 45 seconds, annealing for 45 seconds, and 72°C for 1 minute; a final extension at 72°C for 10 minutes; and holding at 4°C. The amount of cDNA used for each PCR was 20 ng in a 25-μL reaction volume. The PCR products were analyzed by electrophoresis through 1% agarose gel and visualized by ethidium bromide staining. 18S rRNA was used as an internal control.

Toxicology and Biodistribution in Rats and Nonhuman Primates

A good laboratory practice (GLP)–compliant 1- and 3-month dose-based toxicity study of ScAAV2-*P1ND4v2* vector delivered by intravitreal injection into the eyes of normal rodents was performed. The control group (group 1), low-dose group (group 2), medium-dose group (group 3), and high-dose group (group 4) each included 20 rats (10 males, 10 females). Half of each group were euthanized and necropsied at 1 month (30 days) and half at 3 months (90 ± 3 days) after injection, respectively.

We also performed a 3- to 4-month safety and biodistribution study of *P1ND4v2* vector delivered by intravitreal injection into eight normal rhesus macaques. Vector titered at 2.46×10^{11} vg/mL was diluted 1:1 with sterile water to 1.23×10^{11} vg/mL, and 200 μL was vitreally injected for a total dose of 2.46×10^{10} vg ($n = 5$); another group received a higher dose of 2.02×10^{11} vg ($n = 3$). Two animals were euthanized at 3 months (90 days) and one at 4 months (126 days). A fourth animal received bilateral intravitreal injections of balanced salt saline (volume = 200 μL) and was euthanized at 3 months (90 days). Two animals received bilateral injections. In these, the fifth and sixth animals, a total dose of 2.46×10^{10} vg was injected into one eye; the second eye was injected 1 month later, and euthanasia was performed 3 months after the last injection. Three animals that received a higher dose of the test article were euthanized at 3 months (~90 days).

A neutralizing antibody assay was performed on serum samples obtained from the rhesus macaques injected with the test article synthesized at the vector core facility of the University of Florida or at the University of North Carolina. The neutralizing antibody assay was performed according to the modified protocol from Boye et al.[21] Briefly, a self-complementary AAV2(Y444,500,703F)-smCBA-mCherry vector was preincubated with heat-inactivated nonhuman primate (NHP) serum samples at various dilutions, beginning with a 1:5 dilution, followed by serial 1:4 dilutions and ending at 1:20,480. The serum-vector mixtures were used to infect ARPE-19 cells at multiplicity of infection of 1000 vector genomes/cell. Three days post infection, cell viability was confirmed by microscopy and transduction scored by flow cytometry. The expression of mCherry was quantified by multiplying the percentage of cells positive for mCherry by the mean fluorescence intensity. The neutralizing antibody (NAb) titer was reported as the highest serum dilution that inhibited self-complementary AAV2(Y444,500,703F)-smCBA-mCherry transduction > 50%.

In both species, tissue samples were collected in 10% neutral buffered formalin for histopathological analysis, and parallel samples were flash frozen in liquid nitrogen for assessment of vector biodistribution. The injected eye with optic nerve was fixed in Davidson's (rats) or 4% paraformaldehyde (monkeys). Histology and histopathology examination of prepared slides were performed under contract agreement at Charles River Pathology Associates-Illinois. Histopathology analysis was conducted by a board-certified veterinary pathologist (CD) who was masked to study treatments and animal assignment. In addition, genomic DNA (gDNA) was extracted from frozen tissue or blood collected. All other frozen organs were segregated by treatment. The following organs were extracted: skeletal muscle quadriceps, diaphragm, heart, cerebrum, lung, spleen, liver, kidney, pancreas, gonads, jejunum, parotid gland, mesenteric lymph node, and uninjected eye with corresponding optic nerve. DNA was quantified and analyzed by real-time PCR. Typically, 1.0 μg of each DNA sample was assayed in triplicate. Tissues from the day 30 high-dose rat groups were assayed first. If any tissue from at least one animal in this group was positive, that tissue was analyzed in all the day 90 high-dose animals. The algorithm was continued until the tissue was found to be negative. For primates, the presence of vector DNA was assessed.

Investigative Ophthalmology & Visual Science

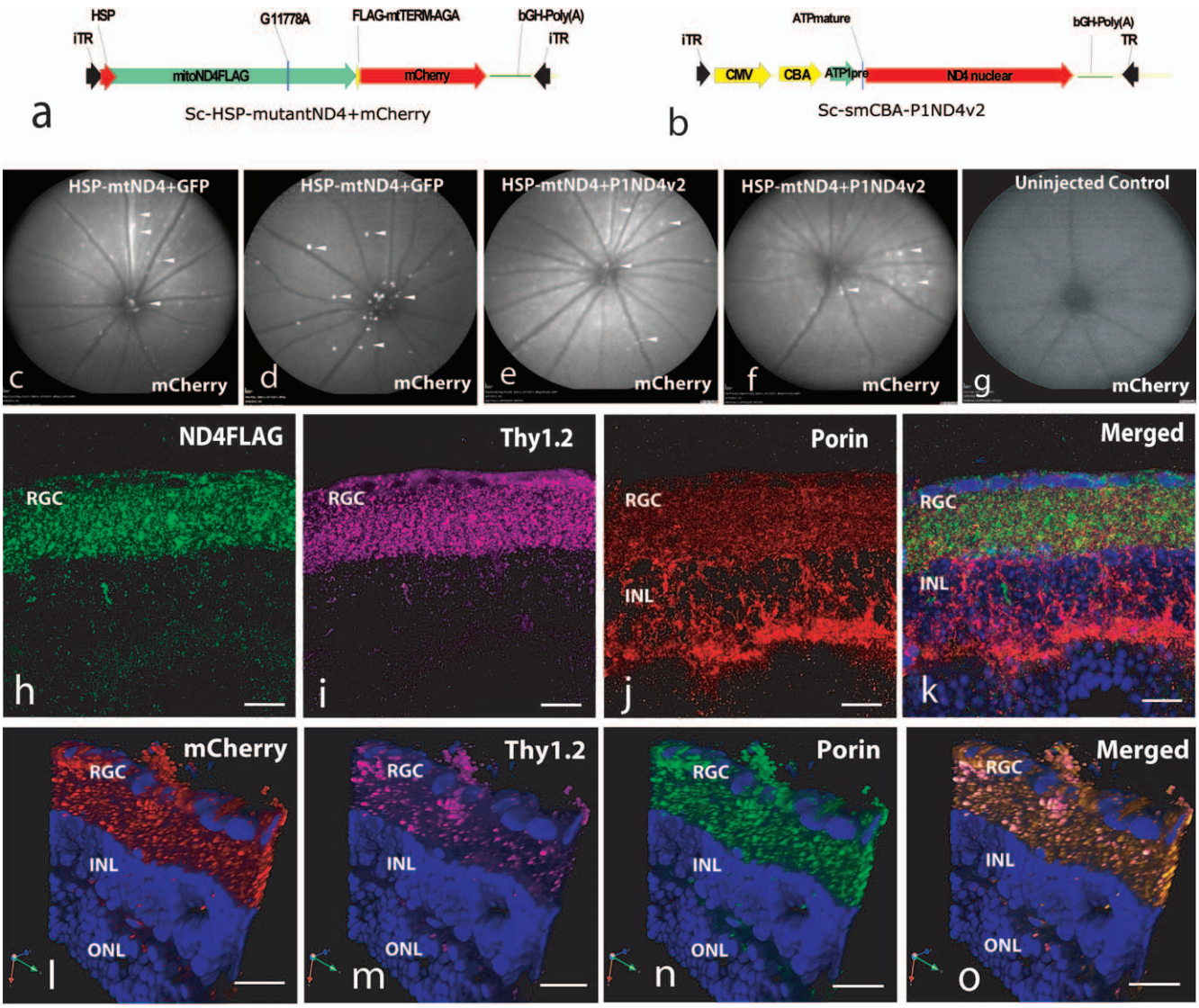

Figure 1. Plasmid maps and expression of mutant ND4. Plasmid maps of (**a**) the mutant mitochondrial *ND4+mCherry* and (**b**) test article, *P1ND4v2*, are shown. Four months after dual viral injections, confocal laser scanning ophthalmoscopy shows mCherry fluorescence (*arrowheads*) in ScAAV2-*GFP*- and ScAAV2-*HSP-ND4(G11778A)+mCherry*-injected eyes (**c**, **d**) and in test article, ScAAV2-*P1ND4v2*-, along with ScAAV2-*HSP-ND4(G11778A)+mCherry*-injected eyes (**e**, **f**). mCherry fluorescence was absent in uninjected control (**g**). Confocal microscopy of retinal flat mounts performed 4 months after injection of ScAAV2-*HSP-ND4(G11778A)+mCherry* shows immunofluorescence of FLAG (**h**), Thy1.2 (**i**), porin (**j**), and merged image of FLAG, porin, and DAPI (**k**). A 3D rendered view of retinal longitudinal sections shows perinuclear mCherry expression (**l**) in RGCs (**m**), mitochondrial porin (**n**), and a merged image of mCherry, Thy1.2, porin, and DAPI (**o**). iTR, inverted terminal repeat; ATP1pre, ATP 1 leader sequence; HSP, mitochondrial heavy strand promoter; ONL, outer nuclear layer; INL, inner nuclear layer; RGC, retinal ganglion cell layer. *Scale bars*: 25 μm.

Antigen-Specific Response Lymphocyte Proliferation Assay

Anti-AAV2-triple tyrosine (Y) to phenylalanine (F) capsid mutant antigen-specific lymphocyte proliferation responses were assessed as previously described.[22] After isolation and purification from blood, lymphocytes were cultured at 1×10^5 cells per well of 96-well plates. Lymphocytes were separated into four groups with three control and six primate sample cultures per group: unstimulated (as negative control) or stimulated with AAV2trpmut (5000, 500, and 50 particles/cell. After 5 days of incubation the stimulation index (SI), defined as the mean counts per minute of [3H]thymidine from stimulated cells divided by the mean counts per minute of [3H]thymidine from unstimulated cells was calculated. Stimulation index values greater than 2.0 to 3.0 are considered significant. The viability of each lymphocyte culture was confirmed by positive controls with mitogen-induced proliferation in response to phytohemagglutinin (PHA) and recall antigen-induced proliferation to *Candida albicans*.

Statistical Analysis

One-way analysis of variance followed by Student's *t*-test was used to compare PERGs and SD-OCT data. The mouse groups compared were age-matched mice uninjected or injected with ScAAV2-*mCherry* (no-disease control) and mice either inoculated with ScAAV2-*HSP-ND4(G11778A)+mCherry* along with the test article, ScAAV2-*P1ND4v2*, or mock treated with ScAAV2-*GFP*. Quantification of cells in the RGC layer and optic nerve axons between the mock-treated and test article–treated mouse groups was determined using unpaired Student's *t*-test.

Investigative Ophthalmology & Visual Science

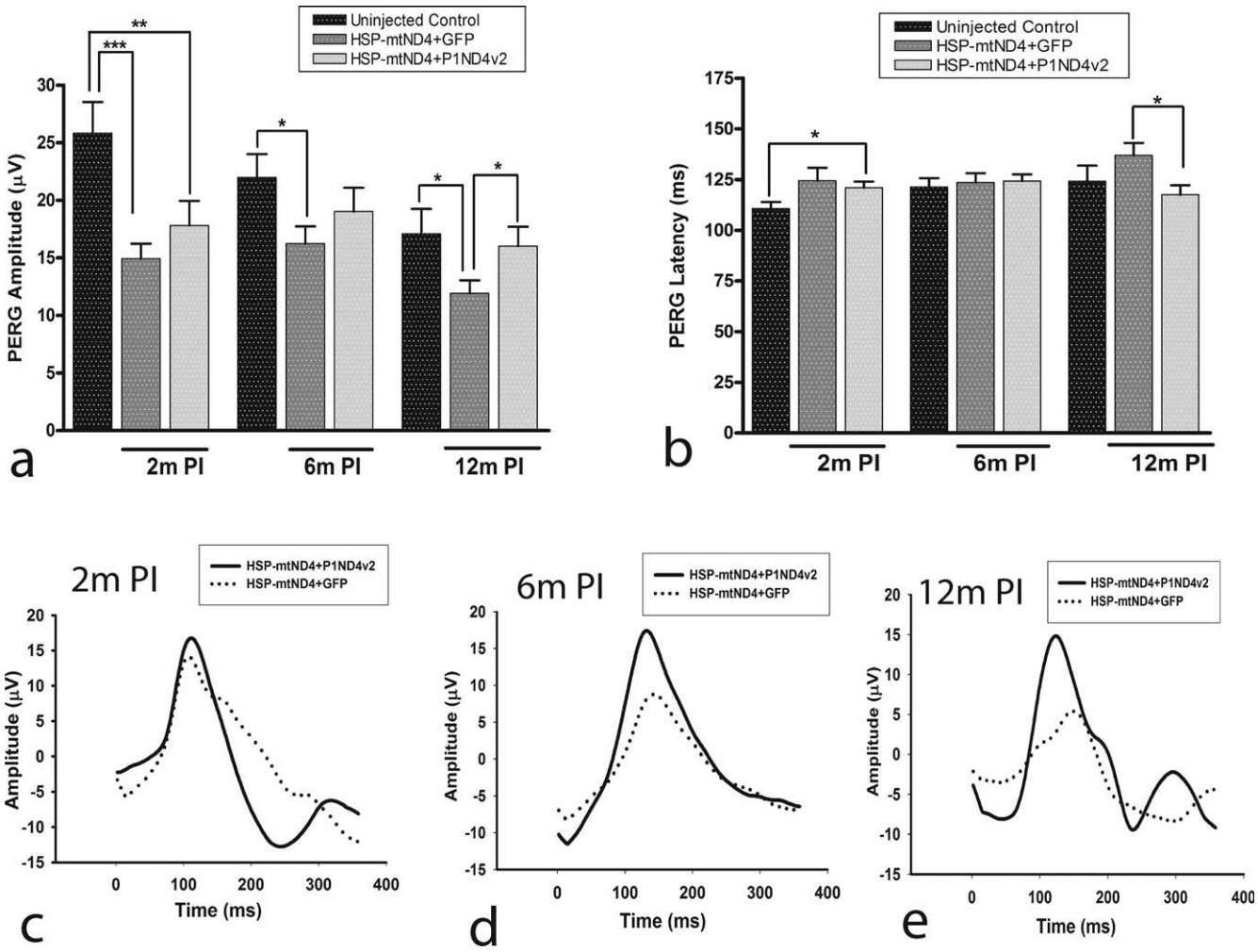

Figure 2. Rescue of visual function. PERG analysis of uninjected age-matched control mice and mice injected with ScAAV2-HSP-ND4*(G11778A)+mCherry* and mock treated with ScAAV2-*GFP* or test article, ScAAV2-*P1ND4v2*, performed at 2 months (2m) 6 months (6m), or 12 months (12m) post injection. *Bar plots* of PERG amplitudes (**a**) and latencies (**b**) are shown (mean ± SE). Representative PERG waveforms are shown at (**c**) 2 months, (**d**) 6 months, and (**e**) 12 months post injection, $n = 24$, $^{*}P = 0.01$ to 0.05, $^{**}P = 0.001$ to 0.01, $^{***}P < 0.001$. m PI, months post injection.

All the results were expressed as mean ± standard error (SE), and P values less than 0.05 were considered statistically significant.

Results

Mutant and Wild-Type ScAAV2-*P1ND4v2* Efficiently Transduces RGCs

For rescue experiments, mice ($n = 20$) were injected in the vitreous with self-complementary AAV2 containing the mutant G11778A *ND4* (ScAAV2-*HSP-ND4G11778AFlag*) and a second gene, *mCherry*, in the mitochondrial genetic code (Fig. 1a) for visualization of transduced organelles. Both genes were driven by a single human HSP. This construct was packaged in mitochondrially targeted AAV virions and injected into both eyes of mice to induce LHON, followed 72 hours later by injections of either ScAAV-*GFP* ($n = 10$) or the test article ScAAV2-*P1ND4v2* (Fig. 1b) ($n = 10$); control mice remained uninjected ($n = 2$). Four months later, mCherry was visualized in the retinas of mock-treated (Figs. 1c, 1d) and test article–treated (Figs. 1e, 1f) live mice and absent in uninjected control mice (Fig. 1g). Confocal microscopy revealed ND4FLAG (Fig. 1h) in RGCs labeled by Thy1.2 (Fig. 1i) colocalized to mitochondria labeled by VDAC/porin (Fig. 1j) in the merged image (Fig. 1k). Red fluorescence (Fig. 1l) in RGC (Fig. 1m) mitochondria (Fig. 1n) confirmed mCherry also expressed in RGC mitochondria (Fig. 1o). Confocal images showed expression of human wild-type ND4 that colocalized to RGC mitochondria (Supplementary Figs. S1a–S1e) absent in negative control (Supplementary Fig. S1f). Semiquantitative real-time PCR showed *P1ND4v2* transcripts exclusively in the ocular tissues and absent in nonocular tissues such as liver, pancreas, and heart (Supplementary Fig. S1g).

Test Article (ScAAV2-*P1ND4v2*) Preserves Visual Function in LHON Mice—PERG Analysis

The PERG, a sensitive measure of visual loss and RGC function, probed the effects of the test article at 2, 6, and 12 months after AAV injections. ANOVA with random effects to account for correlated measurements made on the same animals over time showed a highly significant difference in PERG amplitudes of age-matched uninjected controls, mock-treated, and test article–treated mouse groups ($P = 0.0001$) (Supplementary Table S1); however, there was no statisti-

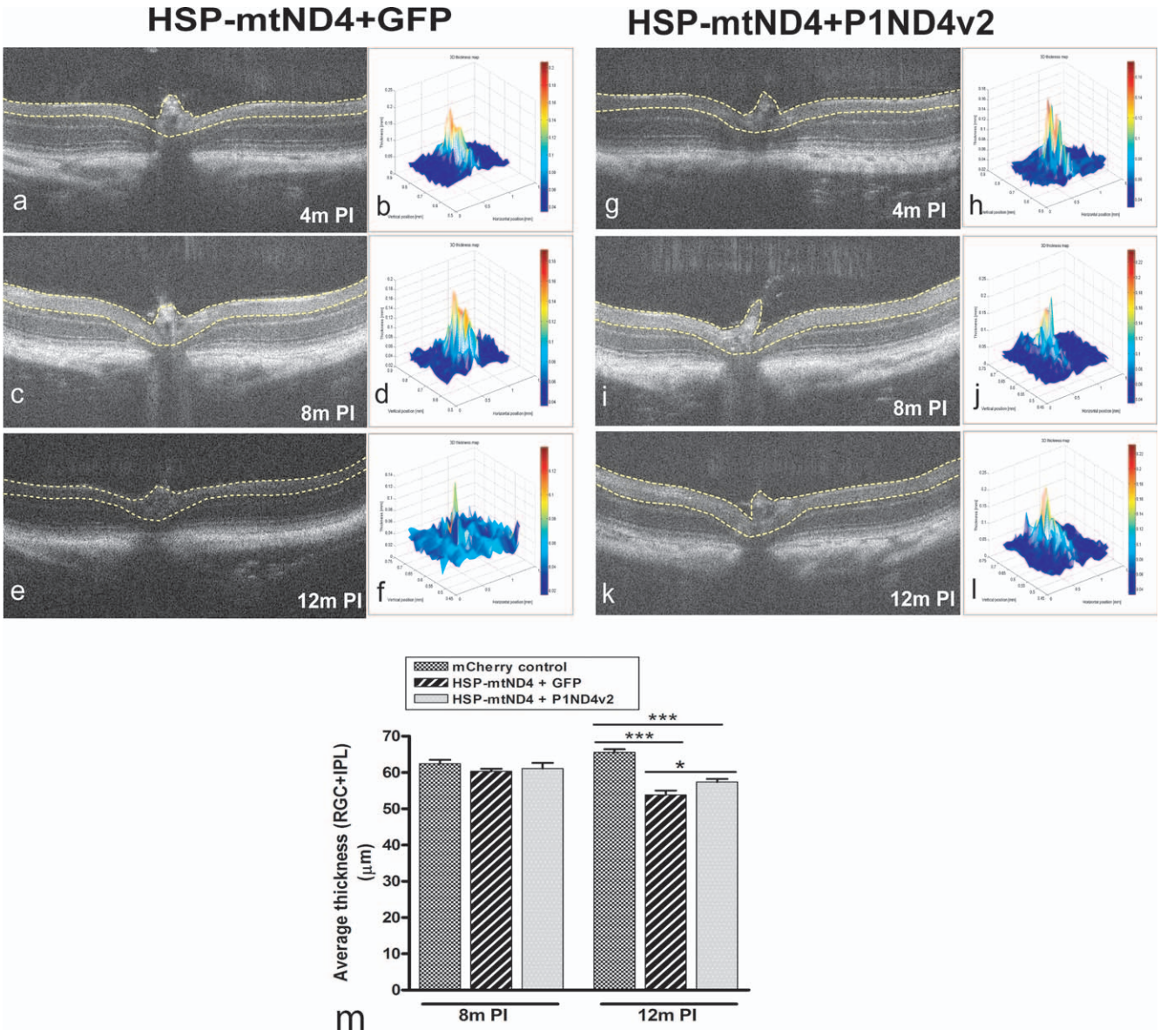

Figure 3. In vivo optical coherence tomography (OCT) imaging. Serial OCT imaging of a mock-treated mouse eye shows the nerve fiber layer to the inner boundary of the inner nuclear layer demarcated by *yellow lines* (**a**) and a corresponding 3D thickness map (**b**) at 4 months PI, a two-dimensional image (2D) (**c**) and 3D map (**d**) at 8 months PI, and a 2D (**e**) and 3D map (**f**) at 12 months PI. Also shown are 2D (**g**) and 3D maps (**h**) of a rescued mouse eye injected with the test article at 4 months PI, 2D (**i**) and 3D maps (**j**) at 8 months PI, and a 2D image (**k**) and 3D map (**l**) at 12 months PI (**m**). The *bar plot* shows average thickness measurements from the nerve fiber layer to the inner boundary of the inner nuclear layer (as marked in the 2D images) at 8 and 12 months PI (mean ± SE); $n = 26$, $^{*}P = 0.01$ to 0.05, $^{***}P < 0.001$. m PI, months post injection.

cally significant difference when the latencies were compared ($P = 0.064$) (Supplementary Table S2). At 2 months post injection, the average PERG amplitudes of test article– and mock-treated mice were significantly reduced compared to those of age-matched uninjected mice (17.8 ± 2.14, 14.94 ± 1.3, and 25.85 ± 2.7 μV; mean ± SE) ($P < 0.05$). However, while the mock-treated mice continued to show significantly reduced amplitude at 6 months, which worsened at 12 months following mutant ND4 injection ($P < 0.05$), the test article–treated mice showed rescue of PERG amplitudes, and the data were comparable to those for the age-matched uninjected mice ($P > 0.05$) (Supplementary Table S1). In addition, the average PERG amplitudes and latencies were significantly rescued in test article–treated mice (16 ± 1.68 μV; 117.5 ± 4.64 ms) compared to the mock-treated mouse group at 12 months post injection (11.9 ± 1.14 μV; 136.9 ± 6.13 ms) ($P < 0.05$) (Supplementary Tables S1, S2). Bar graphs show mean PERG amplitudes (Fig. 2a) and latencies (Fig. 2b). Representative waveforms at 2 (Fig. 2c), 6 (Fig. 2d), and 12 months (Fig. 2e) illustrate that loss of amplitude and delay in latency were suppressed by treatment.

Test Article (ScAAV2-*P1ND4v2*) Preserves the RGC and Inner Plexiform Layers in LHON Mice—SD-OCT Analysis

As measured by SD-OCT, the RGC layer and inner plexiform layers appeared normal in mock-treated eyes of live mice at 4 (Figs. 3a, 3b) and 8 months post injection (Figs. 3c, 3d), but at 12 months these layers atrophied (Figs. 3e, 3f). In mice

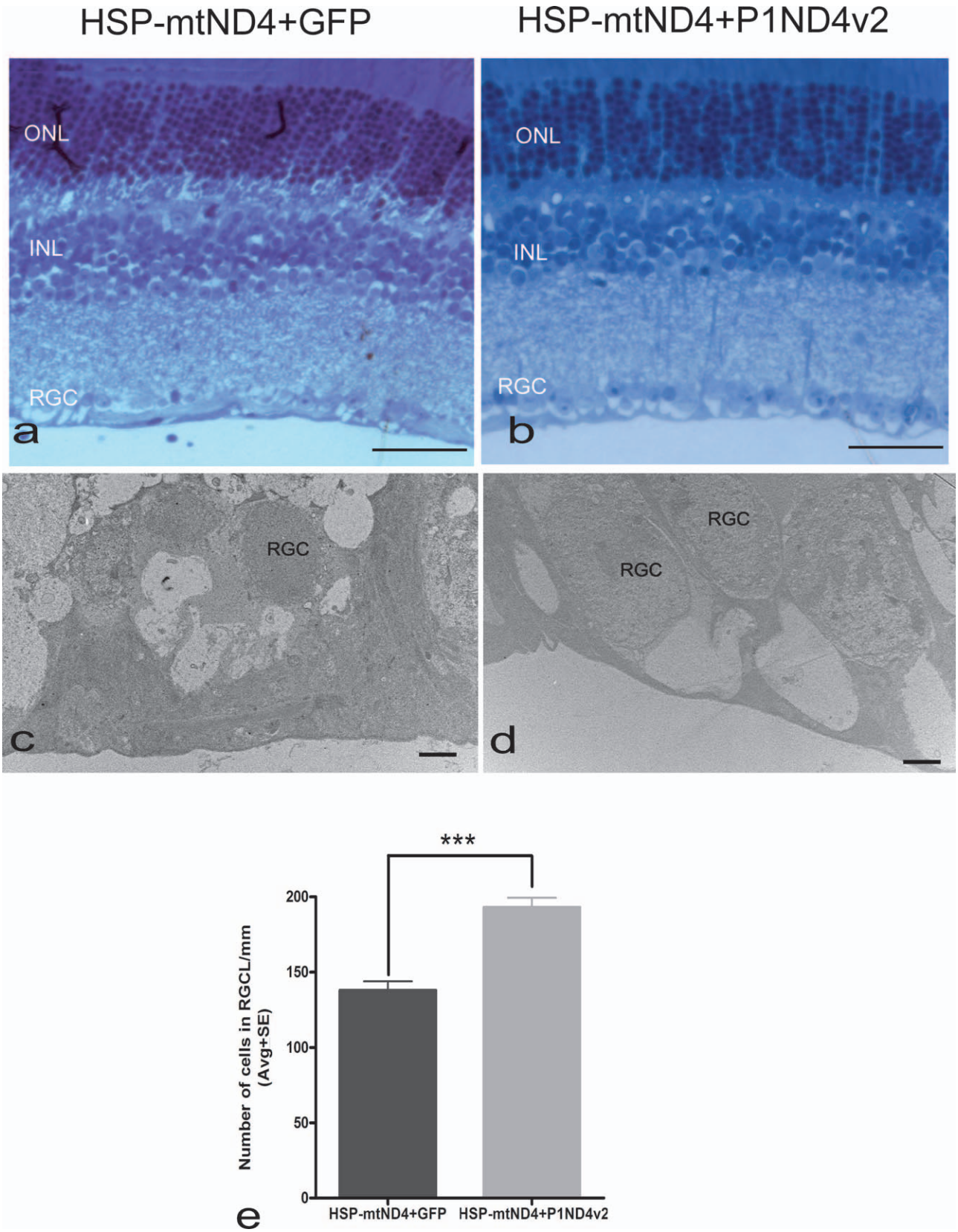

Figure 4. Histological and ultrastructural studies of retina. One year after intravitreal injection, light microscopic analysis of toluidine blue–stained longitudinal retinal sections showed (**a**) loss of RGCs with mock treatment (ScAAV2-*GFP*). (**b**) With ScAAV-*P1ND4v2* rescue from the disease-inducing ScAAV2-HSP-*ND4(G11778A)+mCherry*, there were more RGCs. (**c**) Transmission electron microscopy identified apoptotic RGCs in mock-treated mice. (**d**) Transmission electron micrographs of mice treated with *P1ND4v2* and also injected with ScAAV2-*mtND4FLAG+mCherry* had RGCs with a characteristic elliptical and lighter nucleus typical of RGCs. (**e**) *Bar plot* of RGC numbers counted on toluidine blue–stained light microscopic images is shown (mean ± SE). *Scale bars*: 20 μm (**a**, **b**); 2 μm (**c**, **d**). ONL, outer nuclear layer; INL, inner nuclear layer; RGC, retinal ganglion cell layer. $n = 10$, $^{***}P = 3.65 \times 10^{-5}$.

Investigative Ophthalmology & Visual Science

protected with the test article, these retinal layers were preserved at 4 (Figs. 3g, 3h), 8 (Figs. 3i, 3j), and 12 months (Figs. 3k, 3l). ANOVA with random effects to account for correlated measurements made on the animals over time showed highly significant difference among the mCherry-injected no-disease control, disease-induced mock-treated control, and test article–treated mice ($P < 0.0001$). Compared to the mCherry-injected no-disease control, the mean thickness of either mock-treated or test article–treated control did not show a significant difference at 8 months post injection ($P > 0.05$); however, at 12 months, both the treated groups showed significant difference compared to the no-disease mCherry control group ($P < 0.05$) (Supplementary Table S3). The mean thickness of the inner retina of the mock-treated and test article–treated mice did not show significant difference at 4 months (54.07 ± 0.72 and 56.31 ± 0.79 μm, mean ± SE) and 8 months post injection (60 ± 0.72 and 61.54 ± 1.5 μm, mean ± SE) ($P > 0.05$). However, at 12 months post injection, the test article–treated mice showed a significant rescue of inner retina thickness compared to the mock-treated mice (57.4 ± 0.81 and 53.2 ± 1.19 μm, mean ± SE) ($P < 0.05$) (Supplementary Table S3). Bar graphs show mean inner retina thickness at 8 and 12 months post injection (Fig. 3m).

Test Article (ScAAV2-*P1ND4v2*) Rescues Inner Retinal Layers and Optic Nerves in LHON Mice—Histopathology and Ultrastructural Analysis

One year after intraocular injections, light microscopy confirmed loss of RGCs with mock treatment (Fig. 4a) but more RGCs in rescued eyes (Fig. 4b). Transmission electron micrographs (TEM) revealed apoptotic RGCs with condensed chromatin after mock treatment (Fig. 4c). In contrast, mice rescued with *P1ND4v2* had RGCs with normal elliptical morphology with lighter nucleoplasm (Fig. 4d). Quantitative evaluation of RGCs on toluidine blue–stained light microscope images showed a significantly greater cell number in the mice injected with ScAAV2-*P1ND4v2* (193 ± 6.6/mm, mean ± SE) compared to the ScAAV-*GFP* group (138 ± 5.9/mm, mean ± SE), $P = 8.8 \times 10^{-6}$ (Fig. 4e).

The test article also prevented optic neuropathy. One year after intraocular injections, TEM of optic nerves of mock-treated animals revealed reduced axon density (Fig. 5a), swollen axons with thin myelin lamellae (Fig. 5b), prominent astroglial processes where axons were lost (Fig. 5c), and degenerating axons exhibiting Wallerian degeneration (Fig. 5d). With treatment, axons were more numerous (Fig. 5e). Inflammatory cell phagocytosis of myelin was still evident (Fig. 5f, magnified from Fig. 5e), but astroglial processes and axonal degeneration were less prominent (Figs. 5g, 5h). Axon counts for treated mice were 50% higher (0.203 ± 0.018 axons/μm^2, mean ± SE) relative to mock treatment (0.138 ± 0.013 axons/μm^2), $P = 0.00758$ (Fig. 5i).

Toxicology and Biodistribution Data in Rats and Nonhuman Primates

Histopathologic assessment by a veterinary pathologist masked to study treatment showed a variety of microscopic changes in the rat eye at 30 (Table 1) and 90 days post injection (Table 2), but not in other organs. Lesions were found in the injected eye at a percentage of 30% (6/20) in the control balanced salt solution (BSS) group 1, 35% (7/20) in low-dose group 2, 10% (4/20) in medium-dose group 3, and 40% (8/20) in high-dose group 4. Thus, lesions were not a result of viral infection. Degeneration of the lens with identification of balloon cells

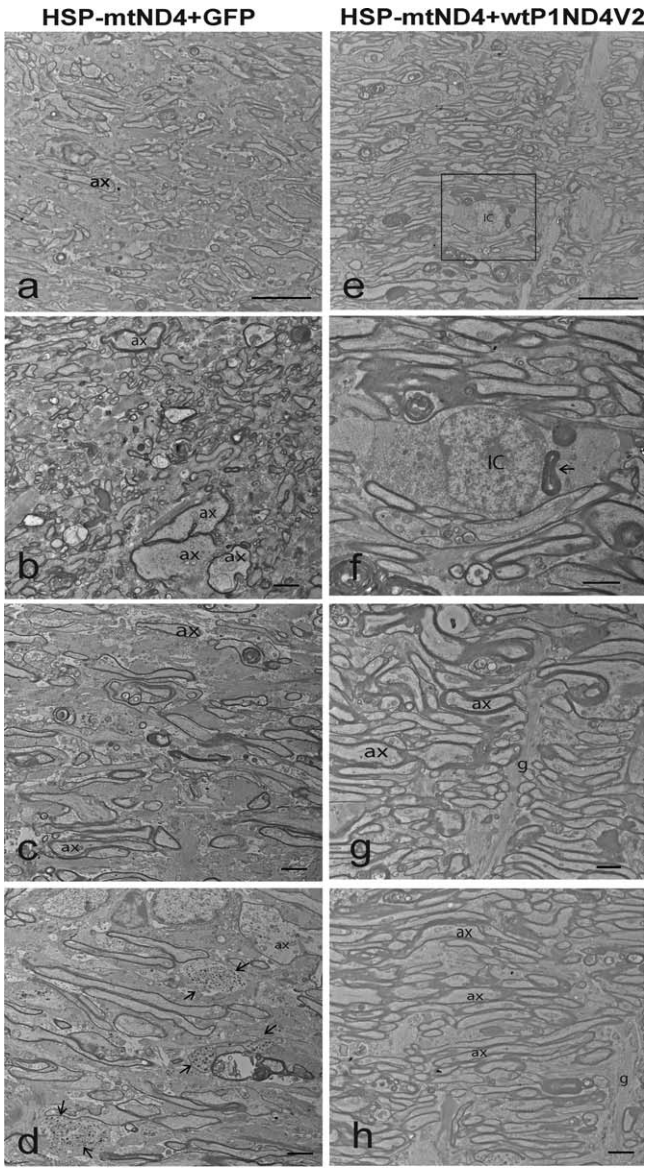

Figure 5. Ultrastructural studies of rescue. Transmission electron micrographs of the (**a**) optic nerves of mock-treated mice with reduced axon density, (**b**) swollen axons with thin myelin lamellae, (**c**) prominent astroglial processes where axons were lost, and (**d**) degenerating axons exhibiting Wallerian degeneration (*arrows*). (**e**) Axons were more numerous with *P1ND4v2* treatment. (**f**) Enlarged image showing an inflammatory cell exhibiting phagocytosis of myelin (*arrow*). (**g**, **h**) Astroglial processes and axonal degeneration were less with *P1ND4v2* treatment. (**i**) *Bar graph* of axon numbers is shown (mean ± SE). *Scale bar*: 25 μm (**a**, **e**); 2 μm (**b**–**d**, **f**–**h**). g, glia; ax, axons; IC, inflammatory cell. $n = 10$, $^{**}P = 0.00758$.

Table 1. Assessment of Histopathology (Rat 30 Day)

	Male				Female			
	Group 1	Group 2	Group 3	Group 4	Group 1	Group 2	Group 3	Group 4
30 Days	0 vg	6.56×10^6 vg, 0.1×	6.56×10^7 vg, 1.0×	1.97×10^8 vg, 3.0×	0 vg	6.56×10^6 vg, 0.1×	6.56×10^7 vg, 1.0×	1.97×10^8 vg, 3.0×
Number of animals	5	5	5	5	5	5	5	5
Brain, cerebrum								
Examined	5	5	5	5	5	5	5	5
No visible lesions	5	5	5	5	5	5	5	5
Eye								
Submitted/examined	5	5	5	5	5	5	5	5
Degeneration; retina	0	3	0	1	0	0	0	1
Minimal	0	1	0	0	0	0	0	0
Mild	0	1	0	1	0	0	0	1
Moderate	0	1	0	0	0	0	0	0
Gland, salivary, parotid								
Examined	5	5	5	5	5	5	5	4
No visible lesions	5	5	5	5	5	5	5	4
Not examined, not present in section	0	0	0	0	0	0	0	1
Vacuolation	0	0	0	0	0	0	0	0
Minimal	0	0	0	0	0	0	0	0
Infiltration, mononuclear cell	0	0	0	0	0	0	0	0
Minimal	0	0	0	0	0	0	0	0
Heart								
Examined	5	5	5	5	5	5	5	5
No visible lesions	5	5	4	4	5	5	5	5
Cardiomyopathy	0	0	1	1	0	0	0	0
Minimal	0	0	1	1	0	0	0	0
Kidney								
Examined	5	5	5	5	5	5	5	5
No visible lesions	5	5	4	5	5	5	5	5
Not examined; insufficient tissue available for evaluation	0	0	0	0	0	0	0	0
Ectasia; tubular	0	0	1	0	0	0	0	0
Minimal	2	1	3	3	0	0	0	0
Infiltration, mononuclear cell	0	0	0	0	0	0	0	0
Minimal	0	0	0	0	0	0	0	0
Liver								
Examined	5	5	5	5	5	5	5	5
No visible lesions	5	5	5	5	5	5	5	4
Infiltration, mixed cell	0	0	0	0	0	0	0	0
Minimal	0	0	0	0	0	0	0	0
Lung								
Examined	5	5	5	5	5	5	5	5
No visible lesions	5	5	5	5	5	5	5	5
Not examined, not present in wet tissues	0	0	0	0	0	0	0	0
Hemorrhage, acute	0	0	0	0	0	0	0	0
Mild	0	0	0	0	0	0	0	0
Lymph node, mesenteric								
Examined	3	4	5	5	3	5	5	3
No visible lesions	3	4	5	5	3	5	5	3
Not examined, not present in section	2	1	0	0	2	0	0	2

Investigative Ophthalmology & Visual Science

Table 1. Continued

	Male				Female			
30 Days	Group 1 0 vg	Group 2 6.56×10^6 vg, 0.1×	Group 3 6.56×10^7 vg, 1.0×	Group 4 1.97×10^8 vg, 3.0×	Group 1 0 vg	Group 2 6.56×10^6 vg, 0.1×	Group 3 6.56×10^7 vg, 1.0×	Group 4 1.97×10^8 vg, 3.0×
Muscle, diaphragm								
Examined	5	5	5	5	5	5	5	5
No visible lesions	5	5	5	5	5	5	5	5
Muscle, quadriceps								
Examined	5	5	5	5	5	5	5	5
No visible lesions	4	4	5	5	4	5	5	5
Infiltration, mononuclear cell	1	1	0	0	1	0	0	0
Minimal	1	1	0	0	1	0	0	0
Mild	0	0	0	0	0	0	0	0
Degeneration, myofiber	0	0	0	0	0	0	0	0
Mild	0	0	0	0	0	0	0	0
Optic nerve								
Examined	2	5	5	5	4	5	4	5
No visible lesions	2	5	5	5	4	5	4	5
Not examined, not found at necropsy	2	0	0	0	0	0	0	0
Not examined, not present in section	2	0	0	0	1	0	1	0
Ovary								
Examined	-	-	-	-	5	5	5	5
No visible lesions	-	-	-	-	5	5	5	5
Not examined, not present in section	-	-	-	-	1	0	0	0
Pancreas								
Examined	5	5	5	5	5	5	5	5
No visible lesions	5	5	5	5	5	5	5	5
Small intestine, jejunum								
Submitted/Examined	5	5	5	5	5	5	5	5
No visible lesions	5	5	5	5	5	5	5	5
Abnormal appearance	0	0	0	0	0	0	0	0
Spleen								
Examined	5	5	5	5	5	5	5	5
No visible lesions	5	5	5	5	5	5	5	5
Testis								
Examined	5	5	5	5	-	-	-	-
No visible lesions	5	5	5	5	-	-	-	-

(consistent with cataract) was old enough to have occurred during the in-life period. Detachment of the retina in one group 2 male (animal 171) also occurred during the in-life period, as there were associated changes in the retinal pigment epithelial cells that are seen with longer-standing separation of the retina. Degeneration of the retina included all rosette formation or disruption of the retinal layers. There was no inflammatory reaction in any animal with a ruptured lens or a lifted (detached) epithelial layer of the cornea—these two findings may be procurement artifacts.

Additional studies showed that intravitreal administration of *P1ND4v2* to rhesus macaques at doses of 2.46×10^{10} vg ($n = 5$)[23] or 2.02×10^{11} vg ($n = 3$) resulted in no vector-induced gross or microscopic abnormalities in the eye or any other body tissues at 3 to 4 months post injection (Supplementary Table S4). Splitting of the outer plexiform layer of the retina seen in some injected and uninjected control eyes was an artifact of postmortem fixation, as it was not evident on OCT imaging performed in life. Biodistribution studies of all major organs of primates and rats were essentially negative ($\leq$100 copies/μg genomic DNA), although a few viral genomes were detected in lymph nodes and the spleen (Supplementary Tables S5, S6). At the higher dose, moderate levels (<1000 vg) of vector genomes were present in the optic nerves of two *P1ND4v2* primate-injected eyes.

Neutralizing AAV Antibodies and Immune Response Assays in Nonhuman Primates

Neutralizing antibodies were evaluated in two groups of primates injected with the test article synthesized from either the University of Florida or the University of North Carolina. In

Table 2. Assessment of Histopathology (Rat 90 Day)

	Male				Female			
	Group 1	Group 2	Group 3	Group 4	Group 1	Group 2	Group 3	Group 4
90 Days	0 vg	6.56×10^6 vg, 0.1×	6.56×10^7 vg, 1.0×	1.97×10^8 vg, 3.0×	0 vg	6.56×10^6 vg, 0.1×	6.56×10^7 vg, 1.0×	1.97×10^8 vg, 3.0×
Number of animals	5	5	5	5	5	5	5	5
Brain, cerebrum								
Examined	5	5	5	5	5	5	5	5
No visible lesions	5	5	5	5	5	5	5	5
Eye								
Submitted/Examined	5	5	5	5	5	5	5	5
No visible lesions	2	3	2	2	5	3	4	5
Degeneration; retina	1	0	1	0	0	1	0	0
Minimal	1	0	1	0	0	1	0	0
Gland, salivary, parotid								
Examined	5	5	5	5	5	5	5	4
No visible lesions	5	4	5	4	5	5	5	4
Not examined, not present in section	0	0	0	0	0	0	0	1
Vacuolation	0	1	0	1	0	0	0	0
Minimal	0	1	0	1	0	0	0	0
Infiltration, mononuclear cell	0	1	0	1	0	0	0	0
Minimal	0	1	0	0	0	0	0	0
Heart								
Examined	5	5	5	5	5	5	5	5
No visible lesions	5	5	5	5	5	5	5	4
Cardiomyopathy	0	0	0	0	0	0	0	1
Minimal	0	0	0	0	0	0	0	1
Kidney								
Examined	5	5	5	4	3	5	5	5
No visible lesions	3	4	2	1	2	4	5	5
Not examined; insufficient tissue available for evaluation	0	0	0	1	2	0	0	0
Ectasia; tubular	2	1	3	3	1	0	0	0
Minimal	2	1	3	3	1	0	0	0
Infiltration, mononuclear cell	0	0	0	0	0	1	0	0
Minimal	0	0	0	0	0	1	0	0
Liver								
Examined	5	5	5	5	5	5	5	5
No visible lesions	5	5	5	5	5	5	5	4
Infiltration, mixed cell	0	0	0	0	0	0	0	1
Minimal	0	0	0	0	0	0	0	1
Lung								
Examined	5	4	5	5	5	5	5	5
No visible lesions	4	4	5	4	5	5	5	5
Not examined, not present in wet tissues	0	1	0	0	0	1	0	0
Hemorrhage, acute	1	0	0	1	0	0	0	0
Mild								
Lymph node, mesenteric								
Examined	5	5	5	5	4	5	5	5
No visible lesions	5	5	5	5	4	5	5	5
Not examined, not present in section	0	0	0	0	1	0	0	0

Investigative Ophthalmology & Visual Science

Table 2. Continued

	Male				Female			
90 Days	Group 1 0 vg	Group 2 6.56×10^6 vg, 0.1×	Group 3 6.56×10^7 vg, 1.0×	Group 4 1.97×10^8 vg, 3.0×	Group 1 0 vg	Group 2 6.56×10^6 vg, 0.1×	Group 3 6.56×10^7 vg, 1.0×	Group 4 1.97×10^8 vg, 3.0×
Muscle, diaphragm								
Examined	5	5	5	5	5	5	5	5
No visible lesions	5	5	5	5	5	5	5	5
Muscle, quadriceps								
Examined	5	5	5	5	5	5	5	5
No visible lesions	4	5	5	4	4	5	5	5
Infiltration, mononuclear cell	1	0	0	1	1	0	0	0
Minimal	1	0	0	0	1	0	0	0
Mild	0	0	0	1	0	0	0	0
Degeneration, myofiber	0	0	0	1	0	0	0	0
Mild	0	0	0	1	0	0	0	0
Optic nerve								
Examined	3	1	3	5	3	2	5	3
No visible lesions	3	1	3	5	3	2	5	3
Not examined, not present in section	2	4	2	0	2	3	0	2
Ovary								
Examined	-	-	-	-	4	5	5	5
No visible lesions	-	-	-	-	4	5	5	5
Not examined, not present in section	-	-	-	-	1	0	0	0
Pancreas								
Examined	5	5	5	5	5	5	5	5
No visible lesions	5	5	5	5	5	5	5	5
Small intestine, jejunum								
Submitted/examined	5	5	5	5	5	5	5	5
No visible lesions	5	5	5	5	5	5	5	5
Abnormal appearance	0	0	0	0	0	0	0	0
Spleen								
Examined	5	5	5	5	5	5	5	5
No visible lesions	5	5	5	5	5	5	5	5
Testis								
Examined	5	5	5	5	-	-	-	-
No visible lesions	5	5	5	5	-	-	-	-

both the primate groups, the NAb was low to absent prior to injection of the test article. In the first group of primates receiving the test article from the University of Florida, titers of NAbs rose after a single intravitreal injection of scAAV-*P1ND4v2* (Supplementary Table S7). In one rhesus macaque (animal 6), NAb titers did not further increase after an injection in the second eye. In another animal (animal 5), titers did increase following the second injection. No significant levels of NAbs were detected in the animal (animal 4) injected with BSS. Interestingly, the primates that received the test article obtained from the University of North Carolina did not show any rise in antibody titers following injections (Supplementary Table S7). The antigen-specific lymphocyte proliferation response to AAV2-triple tyrosine (Y) to phenylalanine (F) capsid modifications (Y444F+Y500F+Y730F) was monitored at baseline and 1 and 3 months post injection on three primate samples. None of the three primates (rhesus 7, rhesus 8, and rhesus 9) showed a significant rise in SI at any time point (Supplementary Table S8).

Discussion

Our results here demonstrated that intravitreal injection of ScAAV2-*P1ND4v2* was well tolerated in normal rodents and nonhuman primates and in a mouse model of LHON caused by mutated G11778A ND4 DNA, where it rescued the hallmark visual loss and optic neuropathy characteristic of LHON. Currently, there is no effective therapy for LHON[7] or any other disease caused by mutated mtDNA.[24] However, extensive research advances have been made over the past years, and one such emerging and exciting approach is termed allotopic expression. Guy et al.[13] were the first group to use this approach with a human ND4 gene to rescue the defects of oxidative phosphorylation in G11778A LHON cells. It was through allotopic expression of the mutant human ND4

(R340H) that we generated the first bona fide animal model of LHON.[14] Ellouze et al.[25] reproduced the LHON rodent model using the electroporation method of allotopic ND4 plasmid delivery with the R340H mutation and then showed transient rescue of visual and RGC loss using wild-type P1ND4 plasmid.

Recently, we showed that AAV-mediated delivery of *P1ND4v2* rescued the LHON pathology caused by a second allotopic AAV containing the defective R340H ND4 allele.[23] In that study we also showed that the wild-type human ND4 (containing a FLAG epitope tag) protein was imported into the mitochondria and integrated into the 45-subunit complex I where it prevented defective ATP synthesis, suppressing visual loss, reducing apoptosis of RGCs, and preventing demise of axons in the optic nerve. Rescue was feasible only when we used a highly efficient self-complementary backbone and packaging with a triple tyrosine to phenylalanine modified AAV vector for gene delivery of wild-type ND4. Moreover, in that study we used a 4:1 ratio of the wild-type scAAV-*P1ND4Flag* to the allotopic mutant R340H *ND4* (ssAAV2-MT-NDFLAG).[23]

To evaluate the potency of the test article in the current study we used a 4:1 ratio of mutant G11778A *ND4* relative to the test article *P1ND4v2*, thus 16-fold less than in our previously published rescue study. Therefore, the current experiments are most comparable to the human scenario where an excess of mutant ND4 DNA is responsible for the phenotype to be rescued.[17,23] This MTS-AAV approach resulted in expression of mutant human ND4 that was translated inside mitochondria, where it resulted in visual loss and optic atrophy in rodents that mimicked the human LHON condition.[17] We performed the test article injections following a 72-hour period of mutant ND4 injections to minimize the immune responses that could occur within 1 to 2 weeks following the first AAV injection, which could be functionally deleterious and might result in transient expression of these transgenes.[26] Intravitreal delivery of our test article allotopically resulted in ND4 expression in RGC mitochondria and rescue of visual function and ameliorated the demise of optic nerve axons consistent with the results obtained using a tagged ND4 vector.[23] Note that the AAV2 vectors carrying wild-type human ND4 (test article) and the mutant human G11778A ND4 mtDNA used in the current study were packaged in the ScAAV2 vectors with triple tyrosine to phenylalanine capsid modifications. Thus, these studies support the potency of the test article in the LHON mouse model.

Using a comprehensive series of analyses, we also found the test article scAAV-*P1ND4v2* to be safe in two different animal species. Our previous analysis of its ocular safety in three nonhuman primates included the absence of structural or functional abnormalities on OCT and multifocal electroretinograms, and ocular histopathology was extended to additional animals here.[23] Here we further evaluated the safety of intravitreal scAAV2-*P1ND4v2* in additional animals and additional tissues and organs of normal rats and nonhuman primates. In-life studies found no vector-related toxicity or serious adverse ocular reactions except for mild delayed transient vitreous inflammation in one of the nine injected primate eyes and transient autofluorescence in another eye.[23] Splitting of the outer retina layers was an artifact of postmortem fixation, as it was not seen on OCT. Again, our results confirm that no local or systemic toxicity was detected in any of the mild-, moderate-, or high-dose groups of rats or moderate- or high-dose groups of nonhuman primates. As the moderate dose was safe in rhesus macaques, we felt it was not necessary to test the lower dose in these animals. The final titer of the sscAAV-*P1ND4v2* GMP vector was not high enough to dose nonhuman primates, as these eyes can tolerate approximately 200 μL intravitreal injection without significantly raising intraocular pressure that could damage the optic nerve.

The spread of AAV vector was limited to the injected eye with no indication of viral spread outside the treated eye of rats and nonhuman primates, although a few viral genomes were detected in lymph nodes and spleen. Animals that received bilateral injections had no increase in adverse ocular reactions or systemic abnormalities when challenged with the second intraocular injection a month after the first, despite the generation of a humoral-mediated response of NAbs against AAV that has been shown to limit expression after a previous intravitreal injection. We feel that the dosages tested in the current preclinical studies support the safety and efficacy of the test article for use in human studies at least at the low and moderate doses tested here. The high levels of NAbs detected in our nonhuman primate studies following intravitreal injection did not pose a safety concern with injection into the second eye, but would likely limit expression of the transgene *P1ND4v2* in the fellow eye.[27]

Introduction of ScAAV2-*P1ND4v2* in G11778A LHON patients could preserve residual visual function and prevent further loss of RGCs and optic nerve axons. The RGC layer exclusively affected in LHON patients can be targeted by optimizing the vector serotype, AAV2, and by choosing the route of vector delivery, intravitreal injection, as we did in our studies.[28,29] Self-complementary vectors that contain positive and negative strands and tyrosine to phenylalanine modifications in the capsid proteins increase the speed and efficiency of transgene expression[30–34] that is relevant to treating LHON patients who have bilateral simultaneous or sequential onset of acute visual loss. While oxidative injury, RGC apoptosis, and axonal loss might already be partially irreversible at this time, gene therapy with a normal human ND4 would be highly relevant to treatment of the symptomatic or presymptomatic eye before significant RGC loss and optic atrophy. We suspect that after safety testing in blind LHON eyes, we will be able to target the asymptomatic fellow eye in those with acute unilateral visual loss before it too goes blind, typically within 6 months. If this is successful, these patients may not have to experience bilateral blindness. Taken together, our studies of safety, efficacy, and biodistribution presented here are a proof of concept for using this test article for our phase I gene therapy clinical trial (NCT02161380) to treat LHON patients with optic neuropathy harboring the G11778A mutation in ND4.

Acknowledgments

Supported by National Eye Institute Grants R24EY018600, R01EY01714, and R01EY123555 (JG), National Institutes of Health (NIH) Grant P30EY014801 (VP), NIH Grant P51OD011092 (Oregon National Primate Research Center Core Grant), and unrestricted grants to the Bascom Palmer Eye Institute and the University of Florida Department of Ophthalmology from Research to Prevent Blindness.

Disclosure: **R. Koilkonda**, None; **H. Yu**, None; **V. Talla**, None; **V. Porciatti**, None; **W.J. Feuer**, None; **W.W. Hauswirth**, AGTC (I), P; **V. Chiodo**, None; **K.E. Erger**, None; **S.L. Boye**, P; **A.S. Lewin**, None; **T.J. Conlon**, None; **L. Renner**, None; **M. Neuringer**, None; **C. Detrisac**, None; **J. Guy**, None

References

1. Pfeffer G, Majamaa K, Turnbull DM, et al. Treatment for mitochondrial disorders. *Cochrane Database Syst Rev.* 2012;4: CD004426.
2. Lam BL, Feuer WJ, Abukhalil F, et al. Leber hereditary optic neuropathy gene therapy clinical trial recruitment: year 1. *Arch Ophthalmol.* 2010;128:1129–1135.

3. Smith KH, Johns DR, Heher KL, et al. Heteroplasmy in Leber's hereditary optic neuropathy. *Arch Ophthalmol*. 1993;111: 1486–1490.
4. Leber T. Uber hereditare und congenital-angelegete Sehnerverleiden. *Graefes Archiv für klinsche und experimentelle Ophthalmologie*. 1871;7:249–291.
5. Riordan-Eva P, Sanders MD, Govan GG, et al. The clinical features of Leber's hereditary optic neuropathy defined by the presence of a pathogenic mitochondrial DNA mutation. *Brain*. 1995;118(pt 2):319–337.
6. Harding AE, Sweeney MG, Govan GG, et al. Pedigree analysis in Leber hereditary optic neuropathy families with a pathogenic mtDNA mutation. *Am J Hum Genet*. 1995;57:77–86.
7. Newman NJ, Biousse V, David R, et al. Prophylaxis for second eye involvement in leber hereditary optic neuropathy: an open-labeled, nonrandomized multicenter trial of topical brimonidine purite. *Am J Ophthalmol*. 2005;140:407–415.
8. Keeney PM, Quigley CK, Dunham LD, et al. Mitochondrial gene therapy augments mitochondrial physiology in a Parkinson's disease cell model. *Hum Gene Ther*. 2009;20: 897–907.
9. Tachibana M, Sparman M, Sritanaudomchai H, et al. Mitochondrial gene replacement in primate offspring and embryonic stem cells. *Nature*. 2009;461:367–372.
10. Glick B, Schatz G. Import of proteins into mitochondria. *Annu Rev Genet*. 1991;25:21–44.
11. Manfredi G, Fu J, Ojaimi J, et al. Rescue of a deficiency in ATP synthesis by transfer of MTATP6, a mitochondrial DNA-encoded gene, to the nucleus. *Nat Genet*. 2002;30:394–399.
12. Neupert W. Protein import into mitochondria. *Annu Rev Biochem*. 1997;66:863–917.
13. Guy J, Qi X, Pallotti F, et al. Rescue of a mitochondrial deficiency causing Leber Hereditary Optic Neuropathy. *Ann Neurol*. 2002;52:534–542.
14. Qi X, Sun L, Lewin AS, et al. The mutant human ND4 subunit of complex I induces optic neuropathy in the mouse. *Invest Ophthalmol Vis Sci*. 2007;48:1–10.
15. Maul GG, Rovera G, Vorbrodt A, et al. Membrane fusion as a mechanism of simian virus 40 entry into different cellular compartments. *J Virol*. 1978;28:936–944.
16. Kaeppel C, Beattie SG, Fronza R, et al. A largely random AAV integration profile after LPLD gene therapy. *Nat Med*. 2013;19: 889–891.
17. Yu H, Ozdemir SS, Koilkonda RD, et al. Mutant NADH dehydrogenase subunit 4 gene delivery to mitochondria by targeting sequence-modified adeno-associated virus induces visual loss and optic atrophy in mice. *Mol Vis*. 2012;18:1668–1683.
18. Yu H, Koilkonda RD, Chou TH, et al. Gene delivery to mitochondria by targeting modified adenoassociated virus suppresses Leber's hereditary optic neuropathy in a mouse model. *Proc Natl Acad Sci U S A*. 2012;109:E1238–E1247.
19. Koilkonda RD, Chou TH, Porciatti V, et al. Induction of rapid and highly efficient expression of the human ND4 complex I subunit in the mouse visual system by self-complementary adeno-associated virus. *Arch Ophthalmol*. 2010;128:876–883.
20. McCarty DM, Fu H, Monahan PE, et al. Adeno-associated virus terminal repeat (TR) mutant generates self-complementary vectors to overcome the rate-limiting step to transduction in vivo. *Gene Ther*. 2003;10:2112–2118.
21. Boye SE, Alexander JJ, Boye SL, et al. The human rhodopsin kinase promoter in an AAV5 vector confers rod- and cone-specific expression in the primate retina. *Hum Gene Ther*. 2012;23:1101–1115.
22. Hauswirth WW, Aleman TS, Kaushal S, et al. Treatment of leber congenital amaurosis due to RPE65 mutations by ocular subretinal injection of adeno-associated virus gene vector: short-term results of a phase I trial. *Hum Gene Ther*. 2008;19: 979–990.
23. Koilkonda RD, Yu H, Chou TH, et al. Safety and effects of the vector for the Leber hereditary optic neuropathy gene therapy clinical trial. *JAMA Ophthalmol*. 2014;132:409–420.
24. DiMauro S, Mancuso M. Mitochondrial diseases: therapeutic approaches. *Biosci Rep*. 2007;27:125–137.
25. Ellouze S, Augustin S, Bouaita A, et al. Optimized allotopic expression of the human mitochondrial ND4 prevents blindness in a rat model of mitochondrial dysfunction. *Am J Hum Genet*. 2008;83:373–387.
26. Zhang YC, Powers M, Wasserfall C, et al. Immunity to adeno-associated virus serotype 2 delivered transgenes imparted by genetic predisposition to autoimmunity. *Gene Ther*. 2004;11: 233–240.
27. Pang JJ, Lauramore A, Deng WT, et al. Comparative analysis of in vivo and in vitro AAV vector transduction in the neonatal mouse retina: effects of serotype and site of administration. *Vision Res*. 2008;48:377–385.
28. Zaiss AK, Muruve DA. Immunity to adeno-associated virus vectors in animals and humans: a continued challenge. *Gene Ther*. 2008;15:808–816.
29. Peden CS, Burger C, Muzyczka N, et al. Circulating anti-wild-type adeno-associated virus type 2 (AAV2) antibodies inhibit recombinant AAV2 (rAAV2)-mediated, but not rAAV5-mediated, gene transfer in the brain. *J Virol*. 2004;78:6344–6359.
30. Zhong L, Li B, Mah CS, et al. Next generation of adeno-associated virus 2 vectors: point mutations in tyrosines lead to high-efficiency transduction at lower doses. *Proc Natl Acad Sci U S A*. 2008;105:7827–7832.
31. Mingozzi F, Maus MV, Hui DJ, et al. CD8(+) T-cell responses to adeno-associated virus capsid in humans. *Nat Med*. 2007;13: 419–422.
32. Zhong L, Li B, Jayandharan G, et al. Tyrosine-phosphorylation of AAV2 vectors and its consequences on viral intracellular trafficking and transgene expression. *Virology*. 2008;381:194–202.
33. Pien GC, Basner-Tschakarjan E, Hui DJ, et al. Capsid antigen presentation flags human hepatocytes for destruction after transduction by adeno-associated viral vectors. *J Clin Invest*. 2009;119:1688–1695.
34. Markusic DM, Herzog RW, Aslanidi GV, et al. High-efficiency transduction and correction of murine hemophilia B using AAV2 vectors devoid of multiple surface-exposed tyrosines. *Mol Ther*. 2010;18:2048–2056.

Investigative Ophthalmology & Visual Science